INTERNATIONAL JOURNAL OF PRECISION ENGINEERING AND MANUFACTURING Vol. 16, No. 6, pp. 1075-1084 JUNE 2015 / 1075
DOI: 10.1007/s12541-015-0139-5 ISSN 2234-7593 (Print) / ISSN 2005-4602 (Online)

A Wirelessly Powered Expanding-Extending Robotic Capsule Endoscope for Human Intestine

Shu He[1,#], Guo-Zheng Yan[1], Quan Ke[1], Zhi-Wu Wang[1], and Wen-Wen Chen[1]

1 Institute of Precise Engineering and Intelligent Microsystems, Shanghai Jiao Tong University, Shanghai, 200240, China
Corresponding Author / E-mail: heshu86@sjtu.edu.cn, TEL: +86-21-34204435, FAX: +86-21-34204434

KEYWORDS: Micro-robot, Gastrointestinal tract, Position detection, Wireless power supply

Instruments for GI diagnostics are increasingly moving toward robotic capsule endoscopes because of their locomotion capabilities. This paper presents a wirelessly powered robotic capsule endoscope that can actively move in the small bowel exploiting the expanding–extending principle. After analyzing the demands of the locomotion, a novel radial motion mechanism with a large expanding/retracting radial ratio was designed, as was an axial motion mechanism with a compact structure. A control system with a special position detector to let the micro-motors avoiding stall state was developed to enhance the stability of the mechanism and reduce the robot's power requirements. The wireless power system enabled the robot to inspect the full length of the intestinal tract. The assembled micro-robot was 14 mm in diameter and 45 mm in length. The maximum anchoring diameter was 32 mm, and the axial telescopic length was 9.5 mm. The test results proved the feasibility of the robot.

Manuscript received: May 12, 2014 / Revised: March 17, 2015 / Accepted: March 25, 2015

1. Introduction

The current clinical methods for diagnosing gastrointestinal (GI) tract disorders are traditional flexible endoscopic techniques; these offer effective and reliable operation in different areas of the GI tract. Flexible endoscopes consist of an actuation cable with a steerable tip that guides the device to the regions of interest, and an external control handle that drives the cable. Because of the rigidity as well as the diameter (from 11 mm up to 13 mm for a standard colonscope) of the cable, the procedure can cause some discomfort or even trauma to patients. Additionally, the cables limit clinicians' ability to image some areas, particularly in the small intestine.[1,2]

In the last few years, growing research interest has focused on the field of minimally invasive and endoluminal devices for surgical and/or diagnostic applications, which promise to improve the treatment of many diseases, especially those that affect the GI tract.[3] Capsule endoscopies, which can be swallowed by patients, were recently introduced.[4-6] They can capture images of the entire GI tract with a micro CMOS/CCD camera and then transmit these wirelessly to outside receiver. Although they are minimally invasive and the diagnostic procedure is painless for patients, there are some obvious functional drawbacks. The main limitation of these devices is that they can move only by exploiting GI peristalsis. In other words, they are unable to accelerate, anchor, or return to regions of interest inside the GI tract. Another drawback is limited working time, which is restricted by the volume of battery. Moreover, capsule endoscopes are characterized by a small diameter, which restricts their ability to expand the GI tract to examine areas concealed within the folds of the collapsed GI tract.

The next generation of devices for digestive tract diagnosis is robotic capsule endoscopes (RCEs), which are capable of active locomotion in the GI tract. Depending on the locomotion mechanism, RCEs fall into one of two categories. The external approach primarily utilizes an external magnetic field that actuates the RCE; the second is onboard approach that utilizes some onboard mechanical devices to drive the RCE.[7] Comparing between the two categories of locomotion mechanism, the advantages of the external approach include a small volume of the RCE and good biocompatibility. However, it is difficult to control the outer magnetic field, especially when the RCE is in the small intestine which is characterized by a tortuous structure.[8-11] By contrast, the onboard approach is easy to control yet uses a complex mechanism.[12-19] Valdastri designed a new mechanism for mesoscale legged locomotion applied in a compliant tubular environment like the GI tract.[17] The device has two sets of legs to expand the intestine to assist with locomotion. Its dimensions match those of commercial capsule endoscopes (11 mm diameter by 25 mm long), but the power

module and the control module are excluded from the robot's body. Moreover, the legs' expansion diameter cannot adjust to variations in intestinal diameter, which might result in failing locomotion in some parts of the intestine characterized by larger or smaller diameters. Our r&d team did a lot of work in this field and developed several prototypes based on bionics. Chen, Lin, Gao designed a type of RCE respectively, whose locomotion were based on the principle of inchworm-like motion.[12,14,16] The RCEs were designed for different district of intestine and possessed different kinds of radial motion mechanisms. Wang presented an RCE based on the principle of earthworm-like motion with diameter of 10 mm and length of 190 mm.[18] Integrating a wireless power supply module in our previously designed RCEs solved the problem of energy supply for extended applications. But there were still some problems existed in these designs like relatively large volume, low movement efficiency of the mechanism, and poor biocompatibility.

This paper describes a novel model of an RCE with an onboard actuating locomotion mechanism that exploited the expanding-extending principle based on bionics to adapt to the intestinal environment. The robot was integrated with two radial motion mechanisms (RMM), an axial motion mechanism (AMM), a video capture module, a control system, and a wireless power system; it measured 14 mm in diameter and 45 mm in length when the AMM was in status of retracting, 54.5 mm when extending. A special kind of expansive mechanism was adopted by the RMM, making the robot obtained a large expanding/retracting radial ratio. The largest expansion diameter of the RMMs was 32 mm, and the ratio of the expansion diameter and retraction diameter reached up to 2.29. Because the expansion diameter of the RMM could adjust with the change of the intestine's diameter, as a result, a larger expansion diameter means that the robot could adapt to the bigger diameter range of the gut, and meanwhile, it is helpful to enhance the anchoring force of the RMM. A mechanical position detector was added into the control system of the robot to improve the security of the motion mechanism, and at the same time, to extend the life of the micro-motors and reduce the energy consumption of the robot system. In addition, the particular wireless power system was designed which took advantage of space without augmenting the diameter or length of the robot. The design of the robot has reference significance to the wireless robotic capsule endoscope and other micro-robots.

2. Design and Analysis of the Mechanism

2.1 Locomotion principle

The intestinal tract is a compliant, nonlinear, viscoelastic cavity covered by a thick (up to 2 mm) layer of lubricating mucus on its internal surface. It has a coefficient of friction on the order of 10^{-3} to 10^{-4}; this makes the locomotion infeasible which exploits effective friction. [20, 21] Inchworm-like locomotion that utilizes the intestinal tract's characteristic of compliance helps the device adapt to the special environment. The simple inchworm-like mechanism consists of two radial motion mechanisms (RMM) for expanding the intestinal tract and an axial motion mechanism (AMM) for the robot's elongation. The locomotion principle is shown in Fig. 1. During step 1, the front RMM

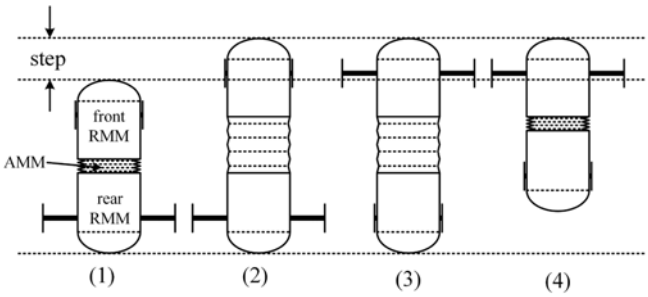

Fig. 1 Principle of inchworm-like locomotion

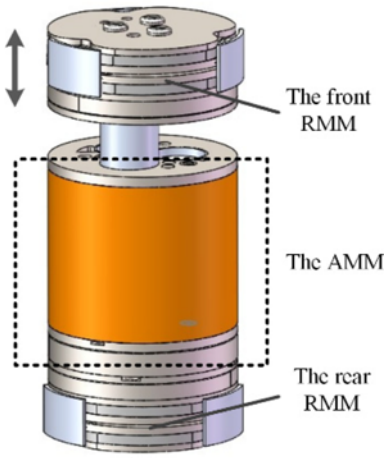

Fig. 2 Mechanical structure of the robot

and the AMM retract while the rear RMM expands to anchor in the intestine. During step 2, the AMM elongates while the rear RMM remains at its previous location and the front RMM moves forward. In step 3, the rear RMM retracts, and the front RMM expands to anchor in the intestine. In step 4, the AMM retracts while the front RMM remains at its previous location and the rear RMM moves forward. Consequently, the whole robot moves forward to complete a step as shown in Fig. 1. If the sequence of the motion gait is inverted, the robot moves backward.

2.2 Mechanical structure of the robot

The robot's mechanical structure comprises two parts as shown in Fig. 2. The front RMM is the front part of the robot; the AMM combined with the rear RMM constitute the rear part of the robot. The two parts are connected by the nut of the AMM and the motor of the front RMM. The three motion mechanisms are actuated by three coreless DC motors. The type of the motor is OT-0412NB-5557RL-15.1-200 with a size of Φ4×12 mm, made by Shen Zhen City Once Top Motor Manufacturing Co., Ltd., Guangdong, China, and the maximum output torque is 0.12 mN·m. The dimensions of the whole mechanism are 14 mm in diameter and 27 mm in length when the three motion mechanisms retracted.

2.3 Design and analysis of the RMM

The structure of the RMM is illustrated in Fig. 3. The RMM is actuated by a coreless DC motor; after the motor, there is a gear reducer to enhance its output torque and slow the rotation speed. The gross reduction ratio of the reducer is 445.7 with 5 levels of gear reduction.

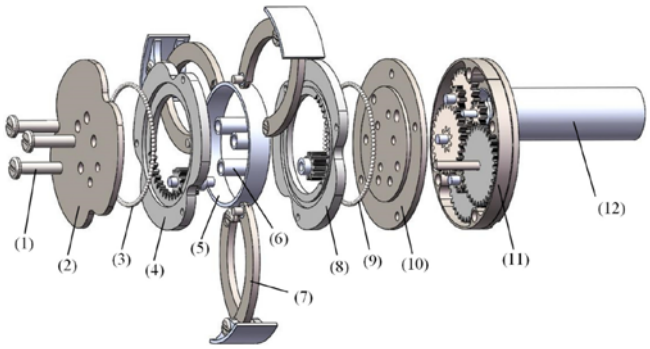

Fig. 3 Exploded view of the RMM: (1) screw set to fix baffle 2 and baffle 10; (2) baffle; (3) balls between baffle 2 and annular gear 4 for friction reduction; (4) annular gear; (5) cylindrical ring between annular gear 4 and annular gear 8 to fix their axial location; (6) sleeve set between baffle 2 and baffle 10 to fix their axial location; (7) three legs; (8) annular gear; (9) balls between annular gear 8 and baffle 10; (10) baffle; (11) gear reducer; (12) coreless DC motor

Fig. 4 The expanding process of the legs

Two meshing 10-teeth gears in the last level of the reducer drive two 43-teeth annular gears rotating oppositely to expand and retract the legs. The leg expanding process is shown in Fig. 4.

Each leg consists of two arc components with ends hinged together; the other two ends are fixed to two annular gears respectively. A curved plate in the end of each leg increases the contact area between the legs and the intestine. This increased contact area could decrease the possibility of intestinal damage from puncture. The curved plate can rotate within a certain range to accommodate intestinal deformations. Three legs form a closed curve to prevent entrapping and injuring intestinal tissue. As shown in Fig. 3, the teeth of the annular gear are incomplete to restrict the open extent of the legs, because there is an extra degree of freedom for the leg if its two ends which are fixed on the annular gear are in the same axial point leading that the legs could rotate at this moment, and it's not allowed with regard to the robot. The maximum expanding diameter of the leg is limited to 32 mm.

Force analysis of the RMM is shown in Fig. 5. Point O is the center of the annular gear, point A is one of the leg's ends (fixed to annular gear), point B is the other one, and point D is the top of the leg. F_a and F_b are the force experienced by the leg at points A and B, respectively caused by the rotation of the annular gears. F_d is the force in point D, and it is the force to expand the intestine. Thus,

$$F_d = (F_a + F_b)\sin\beta \tag{1}$$

According to the mechanical structure,

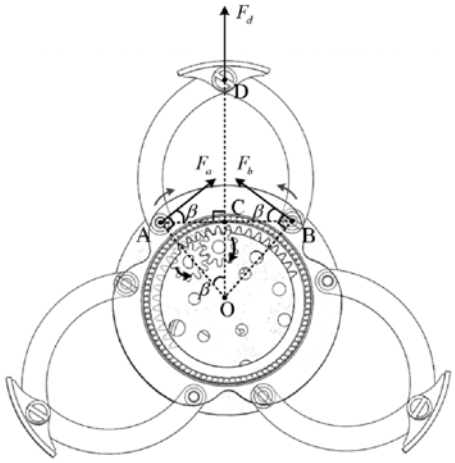

Fig. 5 Force analysis of the RMM

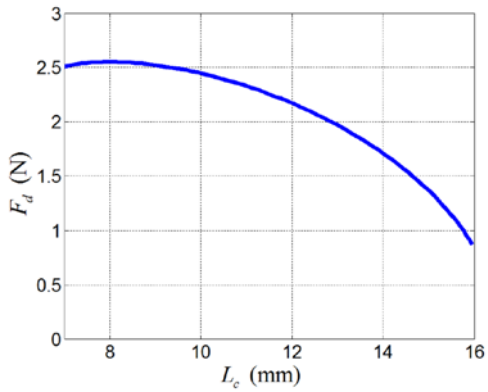

Fig. 6 Relationship between L_c and F_d

$$\begin{cases} \dfrac{T_a}{\eta_a} + \dfrac{T_b}{\eta_b} = T_{motor} \cdot n_{RMM} \\ T_b = \dfrac{\eta_b}{\eta_a} T_a \end{cases} \tag{2}$$

T_a and T_b are output torques of the corresponding gears in Fig. 5, and T_a=3$F_a r_c$, T_b=3$F_b r_c$. r_c is the length of segment OA, T_{motor} is the torque of the coreless DC motor, n_{RMM} is the gross reduction ratio of the reducer, and η_a and η_b are transmission efficiency from the motor to point A and point B, respectively. As the annular gear on which point A is fixed is the former gear, η_b is smaller than η_a because of a more level of gear transmission. According to the above analysis,

$$\begin{cases} F_a = \dfrac{T_{motor} \cdot n_{RMM} \cdot \eta_a}{6 \cdot r_c} \\ F_b = \dfrac{T_{motor} \cdot n_{RMM} \cdot \eta_b}{6 \cdot r_c} \end{cases} \tag{3}$$

Through Fig. 5, the following equation could be deduced.

$$L_c = |CD| + r_c \cdot \cos\beta + L_{wp} \tag{4}$$

Eq. (4) illustrates the relationship between expanding radius L_c and angle β; L_{wp} is the thickness of the work piece outside point D. The length of CD is

$$|CD| = \sqrt{L_{leg}^2 - (r_c \cdot \sin\beta)^2} \tag{5}$$

Table 1 Design parameters of RMM

Symbol	Description	Value
r_c	Length of OA or OB	6.25 mm
n_{RMM}	Gross reduction ratio of the RMM's reducer	445.7
η_a	Transmission efficiency from motor to point A	0.98^5
η_b	Transmission efficiency from motor to point B	0.98^6
β	Rotate angle	20°~100
L_{wp}	The thickness of work piece outside the point D	0.75 mm
L_{leg}	The length of AD	9.58 mm

Table 2 Design parameters of AMM

Symbol	Description	Value
d	Nominal diameter of the screw	1.2 mm
d_2	Pitch diameter of the thread of the screw	1.038 mm
d_1	Minor diameter of the thread of the screw	0.929 mm
P	Thread pitch of the screw	0.25 mm
s	Number of leads of the screw	1
ψ	Lead angle of the screw	4.388
φ_v	Equivalent friction angle of the screw	9.8262
α	Cross-section angle of the thread	60
f	Coefficient of friction between screw and nut	0.15
a	Eccentric distance between screw and output point	4.35 mm
b	Height of the nut	1.5 mm
n_{AMM}	Gross reduction ratio of the AMM's reducer	25.5
η_{ac}	Transmission efficiency of the AMM's reducer	0.98^4

L_{leg} is the length of AD. The design parameters of the RMM are listed in Table 1. The relationship between L_c and F_d is shown in Fig. 6. From the curve, we can observe that F_d climbs up in the first millimeter of the legs' expanding and then declines. A relatively large force occurs when the leg is first beginning to expand, and the maximum force is 2.55 N when the radius of the legs expanded to 8 mm. When L_c expands to 16 mm, F_d is about 0.9 N.

2.4 Design and analysis of the AMM

The proposed AMM is shown in Fig. 7. It is actuated by a coreless DC motor; after the motor is a gear reducer to enhance the output torque. A screw-nut mechanism translates the rotation motion into rectilinear motion after the gear reducer. In order to make use of the available space most efficiently, the motor of the front RMM is fixed on the nut acting as a guide shaft. In the middle part of the AMM, all components are concentrated in a 10.2 mm diameter circle; the toroidal magnetic core and the receiving coil of the wireless power system use the remaining space. The special design could save several millimeters of length compared to designs that position the wireless power system in the end of robot.[14,16] Additionally, this design does not increase the robot's diameter.

Because the output point is partial to the nut, the relationship between the friction torque of the lead-screw mechanism T_f and output force F_{AMM} is given by the standard screw equation:

$$T_f = F_{AMM}\frac{d_2}{2}\left[\tan(\psi+\varphi_v)+\frac{f\pi a}{b\sin\alpha}\right] \quad (6)$$

Where d_2 is the pitch diameter of the screw's thread, ψ is the lead angle of the screw, φ_v is the equivalent friction angle of the screw, f is the coefficient of friction between the screw and the nut, a is the eccentric distance between the screw and the output point, b is the height of the nut, and α is the cross-section angle of the thread. T_f can also be obtained by:

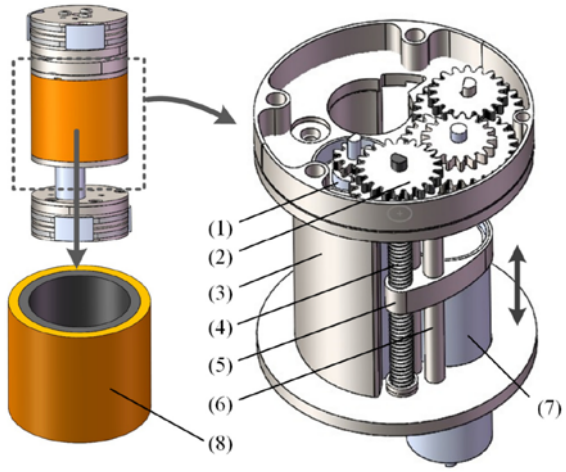

Fig. 7 Structure of the AMM: (1) coreless DC motor; (2) gear reducer; (3) fixed block; (4) lead-screw; (5) nut; (6) guide rod; (7) coreless DC motor of the front RMM; (8) magnetic core and receiving coil of wireless power system

$$T_f = \eta_{ac}\cdot n_{AMM}\cdot T_{motor} \quad (7)$$

Where η_{ac} and n_{AMM} are the efficiency and reduction ratio of the gear reducer of the AMM, respectively. The design parameters of the AMM are listed in Table 2. We calculate that the maximum F_{AMM} is 2.97 N. According to the parameters of the screw and motor, the nut can move at a speed of 4.25 mm/s under a normal load. The maximum length that the AMM could extend is 10.5 mm. To do so, the AMM needs 2.47s to extend completely (under a normal load).

3. Power and Control System of the Robot

3.1 Wireless power system

Because the energy consumed by onboard actuated robotic endoscopes is much greater than that consumed by wireless capsule endoscopes, onboard actuated robotic endoscopes should not be powered by batteries in the present situation. We adopted a wireless power supply system to resolve the power problems of the robot. The wireless power system consisted of a transmitting module and a receiving module, each of which had a coil. Based on electromagnetic coupling principles, power was transmitted between the two coils. Fig. 8(a) shows a transmitting module. The diameter of the coil was 50 cm, and the coil worked at a frequency of 218 kHz. To reduce the internal resistance of the transmitting circuit and enhance the transmitting power, the transmitting coil resonated with an adjustable capacitor. Fig. 8(b) is a magnetic core with a 10.3 mm inner diameter, 1 mm thickness, and 10.4 mm height. It was composed of high permeability ferrite material with an initial permeability of 7k at frequency of 218 kHz to increase coupling efficiency between the transmitting and receiving coils. Fig. 8(d) shows the robot after the wound receiving coil was added. A capacitor was added to resonate with the receiving coil at a

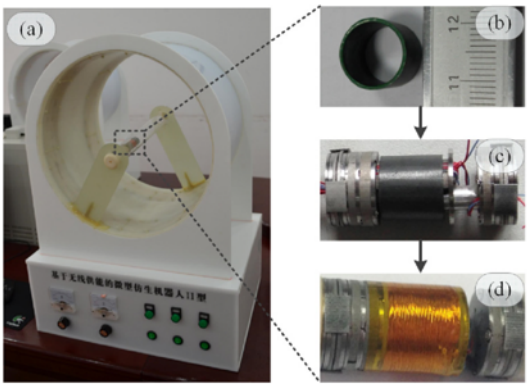

Fig. 8 Wireless power system: (a) power transmitting module; (b) magnetic core; (c) robot with a magnetic core; (d) robot after the wound receiving coil was added

frequency of 218 kHz to decrease the inner resistance of the receiving circuit. When the transmitting coil's transmission power was 30 W, the receiving coil received about 600 mW when at the center of the transmitting coil. The power transmission efficiency was around 2%.

3.2 Position detector

Controlling the motors of the robot is the core task in the whole control system. In our previous work,[12,14,16] we did so by current feedback of the running motor. If the current exceeded a preset value, the motor stopped running. In the actual situation, there are two kinds of overcurrent. The first case occurs when the robot encounters intestinal resistance when a motion mechanism is opening. In this situation, because of the intestinal characteristics of soft and deformable, the current increases gradually; thus, the micro controller could stop the motor before the current rises to the level of stall current. The second case occurs when a motion mechanism is approaching the end of route and encountering mechanical resistance; in this situation, the current would rise to the stall current instantly because the mechanism's materials are very rigid. The first case is related to intestinal safety; and the force acting on the intestine could be adjusted by changing the overcurrent value (preset in the commands). But the second case could harm the robot for the following reasons:

(1) If it works in the stall state frequently, the motor's lifespan and, by extension, the robot's lifespan, could be decreased.

(2) When the motor is in the stall state, the impulsion force exerted on the mechanism is large. This could lead to deadlock of the mechanism, also affecting its lifespan.

(3) Because the stall current is nearly double that of the normal current, it would increase the robot's energy consumption. If the robot is utilizing the wireless power system, it would also lower the voltage, which may result in malfunction of the control system.

For these reasons, avoiding the second type of overcurrent situation is crucial. So, in our new designed control system, we used current feedback to capture intestinal resistance for intestine safety and position feedback to capture mechanical position information for avoiding motor stall.

We designed a position detector to achieve this goal. Fig. 9 shows the position detection method of the RMM which comprises three terminal points. One is a piece of shrapnel (F_{com} in Fig. 9) made by

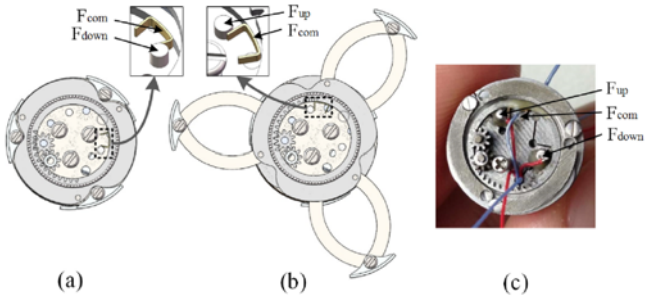

Fig. 9 Position detector of the RMM

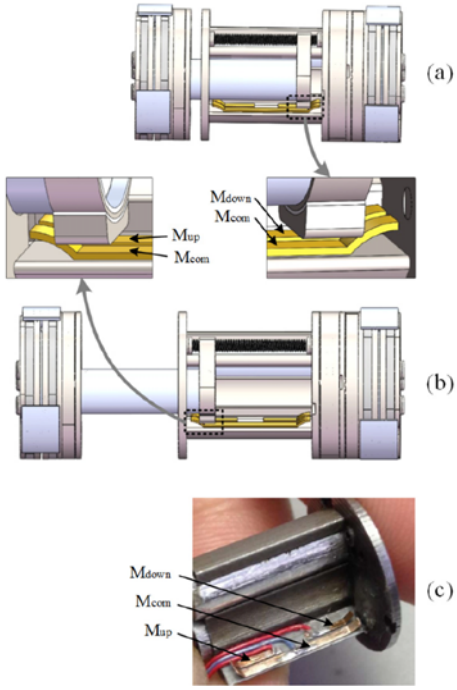

Fig. 10 Position detector of the AMM

phosphor copper with a thickness of 0.1 mm; it is fixed on the annular gear 8 of the RMM (see Fig. 3). Another two terminal points (F_{up} and F_{down} in Fig. 9) comprise a copper pillar 1.2 mm in diameter and 1 mm in height. They are fixed on the baffle 10 of the RMM (shown in Fig. 3). Each terminal point is insulated to its fixture.

In terms of the electrical connection, point F_{com} is connected to a high voltage level of the control circuit board. The other two points are connected to an I/O port of the micro controller, and their voltage is low at the situation of untouching with point F_{com}. In Fig. 9(a), point F_{down} comes into contact with point F_{com} a little before the RMM closes completely. Then the voltage of point F_{down} changes to a high level, and the micro controller could stop the motor before it stalls. Fig. 9(b) shows the opening situation of the position detector. Fig. 9(c) is a picture of the real device.

Fig. 10 shows the position detection scheme of the AMM. It contains three pieces of shrapnels composed of phosphor copper with a thickness of 0.1 mm and a flat plate constructed of stainless steel. Three shrapnels are fastened to fixed block 3 of the AMM (shown in Fig. 7) after insulation processing, and the flat plate is fixed to the nut of the AMM. Fig. 10(a) shows the moment when the flat plate comes into contact with both the M_{down} and M_{com} shrapnels, making them short-current. Fig. 10(b) is the moment when the flat plate comes into

contact with both the M_{up} and M_{com} shrapnels, also making them short-current. The electrical connection is the same as that of the RMM's position detector. Therefore, the above-mentioned two moments will result in a voltage level change, and the micro controller can stop the motor at the two moments.

According to the robot we designed, there are three position detectors worked for three motion mechanisms, therefore there are nine terminal points at all in these position detectors. Point F_{com}, F_{up}, and F_{down} are terminal points in the front RMM, Point R_{com}, R_{up}, and R_{down} are terminal points in the rear RMM, Point M_{com}, M_{up}, and M_{down} are terminal points in the middle part of the robot for AMM.

3.3 Control system

To control the robot remotely and ensure its gait functions properly without harming the intestine, we designed a control system with internal and external components relative to the robot. As shown in Fig. 11, the external components includes an upper computer and a human-computer interface (HMI), an external communication box, a portable video receiver, and a wireless power transmitting module. Commands being input by an operator through HMI are transmitted to the external communication box via serial communication, and are then transmitted to the robot wirelessly. The internal components of the control system include a micro controller unit (MCU), a communication module (Tx/Rx), three motor drivers, a camera driver, a current detector (C detector), and a voltage detector (V detector). When the communication module receives commands, the micro controller will initiate operations based on these commands. If the commands are to drive the motor and execute a gait, the current detector and position detector will monitor the motion of the mechanism simultaneously until the current exceeds the preset overcurrent value or the mechanism runs to the appointed location. The commands may assign the gait of the robot, such as going forward or backward continuously, prompting a single action, or stopping motion. The overcurrent value and overcurrent time can also be set, and the operator can decide whether the camera is functioning. Fig. 11 shows the control system as well as the directions and methods of information transmission.

We chose PIC24F16KM102 (Microchip Technology Inc.) as the micro controller because it has up to 24 I/O interfaces, abundant peripheral functions, and faster processing speed. It includes a serial peripheral interface to communicate with the wireless communication chip SI4455 (Silicon Labs). The communication chip was chosen because of its larger transmitting and receiving power (up to +13dBm) compared to the previously used chip (SI4421, Silicon Labs). It enhanced communication in the high-intensity magnetic field generated by the wireless power system, and its small volume (20-Pin 3×3 mm QFN) was beneficial for our application. We selected 433MHz frequency for communication; this is one of the frequency bands reserved for ISM. Two AT5550 (Aimtron) with independent two-channel low-saturation, low-voltage H-bridge in every chip were used as motor and camera drivers. The maximum output current was up to 800 mA, which was sufficient for our application. The model of the current detective chip was MAX4173F (Maxim Integrated). It is a low-cost, precision, high-side current-sense amplifier with a tiny SOT23-6 package. The circuit board in the robot was a circular board with a diameter of 13.5 mm and thickness

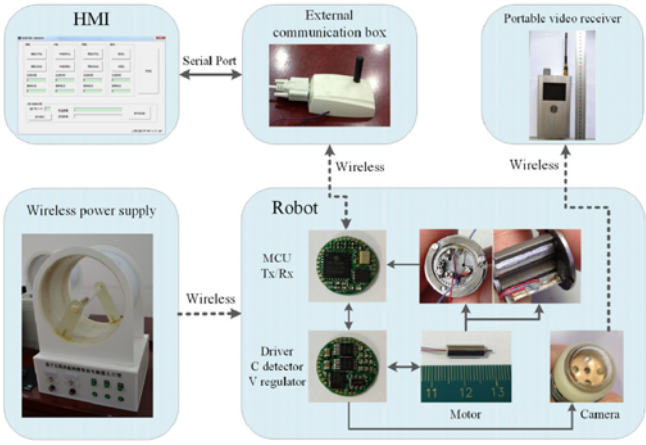

Fig. 11 Block diagram of the control system

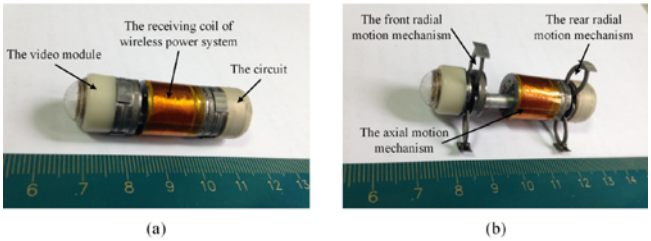

Fig. 12 Prototype of the robot

of 2.8 mm; it was placed in the rear of the robot with a shielding case made by copper to shield it from electromagnetic interference. Its two sides are shown in Fig. 11.

4. Experimental Results

4.1 Mechanism tests

The prototype of the robot is shown in Fig. 12. The diameter of the robot body was 14 mm, and when the AMM was in a retracting state, the length of the robot was 45 mm including the video module in the front and the circuit board at the rear. The design of the front-end and back-end of the robot underwent a streamlining processing to reduce resistance in the intestine. The telescopic length of the AMM was 9.5 mm, which was 1 mm shorter than the design value because of the position detector. The largest anchoring diameter that the RMM could reach was 32 mm. The assembled robot comprised more than 180 high-precision components and weighed 22.43 grams.

In order to ensure that the prototype mechanism's performance would be consistent with its target performance, we conducted a set of experiments. Fig. 13(a) shows the equipment to measure the expanding force of the RMM. The robot was clamped by a vise that was connected to an immotile box to ensure it remained stationary. A dynamometer (FGC-0.5B, Shimpo, Japan) was fastened on a fixed workbench, and its measuring pole was collinear with the line along which one of the RMM's legs expanded. When we sent commands for the robot to open its front RMM, the leg expanded and pressed the plane of measurement. The expanded length of the leg was preset by adjusting the distance between the robot and the dynamometer. The measuring data were transmitted to the PC through a cable, and the expanded length of the leg was measured by a vernier caliper.

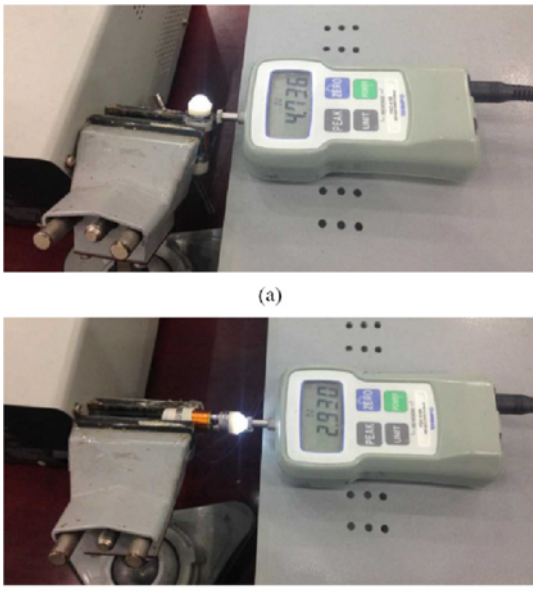

Fig. 13 Mechanism tests

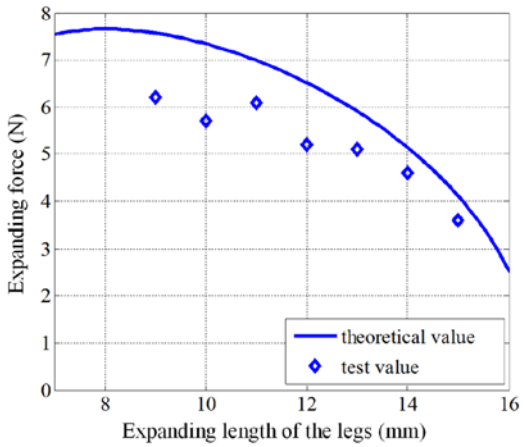

Fig. 14 Comparison between theoretical and test values of the expanding force of legs

The test value and the theoretical value are shown in Fig. 14. Because of friction and other wastage of the mechanism, the test value was slightly lower than the theoretical one, but the trend was the same as that in the theoretical analysis. The efficiency was 75% to 85%.

Fig. 13(b) shows the device for measuring the push force of the AMM. It was similar to Fig. 13(a) except that the robot was clamped horizontally. The average test value of the push force was 2.88 N, which was close to the theoretical one.

4.2 Anchoring force test

Anchoring force is the axial force experienced by the RMM when it is in the status of expanding in the intestine. It is essential to the locomotion of the robot because a precondition for effective locomotion is that the anchoring force is remarkably larger than the axial force experienced by robot body. We designed an experimental platform, which is shown in Fig. 15(c), for researching the characteristics of the anchoring force. A section of the intestine obtained from a 60 kg pig was put on a flat board with one end of the intestine fixed on it with

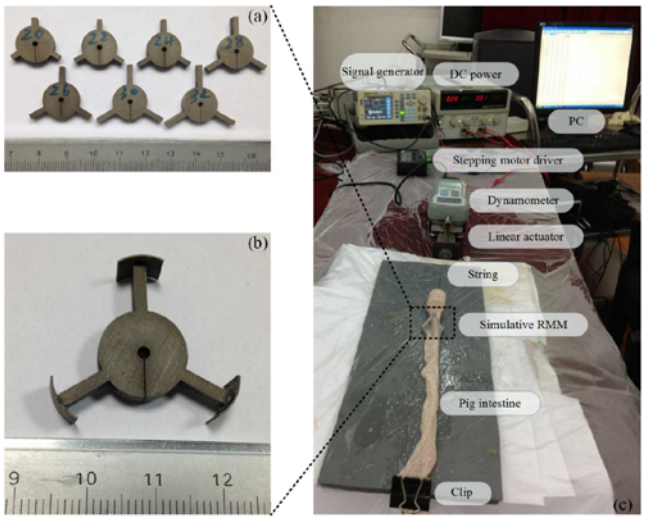

Fig. 15 Anchoring force test platform and devices

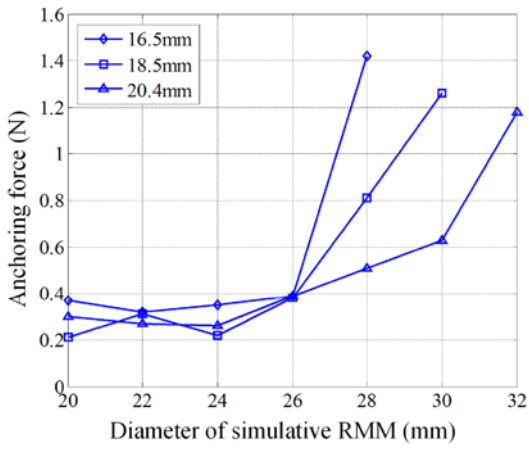

Fig. 16 Anchoring force test results

a clip. A simulative RMM was put into the intestine concentrically with a string connecting it to a dynamometer. The dynamometer was fixed on a linear actuator driven by a stepping motor, and the speed of the linear actuator could be adjusted by different frequency of the square wave trigged by the signal generator shown in Fig. 15(c). In order to imitate the real robot, the speed of the linear actuator was set at 4.48 mm/s. When the linear actuator began working and dragged the simulative RMM, the dynamometer recorded the drag force data automatically. At the same time, we monitored the situation of the simulative RMM and the intestine. If a relative motion was observed between them, we noted the force data at that moment; this was the maximum anchoring force at that status.

The simulative RMM is shown in Fig. 15(b). It consisted of a cylinder with three protruded legs as shown in Fig. 15(a), and three curved plates were fixed on the ends of the legs. The numbers marked on the cylinders were their anchoring diameters. There were 7 different lengths from 20 mm to 32 mm to simulate the expanding procedure of the RMM.

Three different diameters of intestine were tested in this experiment: 16.6 mm, 18.5 mm, and 20.4 mm. The experimental results are shown in Fig. 16. Based on the curves, we arrived at the following conclusions:

(1) When the anchoring diameter was small (less than or equal to 26 mm), the anchoring force was between 0.2 N and 0.4 N, which was close to the force experienced by robot body, and that would lead to invalid anchor of the RMM. Also in this interval of anchoring diameter, the anchoring force did not vary consistently with the diameter of the intestine, which means the major influence factor to anchoring force was not the intestinal diameter in this interval.

(2) When the anchoring diameter was 10 mm more than the intestinal diameter, the anchoring force increased rapidly to more than 1 N with increasing anchoring diameter. Through the analysis of the data, we could infer that the valid anchor of the RMM could be reached if the diameter of the RMM arrived to this extent.

Because there is an inflexion of the anchoring diameter before which the anchoring force varies slightly but after which it augments greatly, the anchoring diameter of the robot should be greater than the inflexion diameter to ensure effective anchor of the RMM.

4.3 Locomotion test

A set of experiments were carried out to verify the locomotion performance of the robot. In the first step, we employed a flexible pipe made of polypropylene casting film to imitate the environment of the intestine. The film's thickness was 40 μm, and the diameter of the pipe was 26 mm. As shown in Fig. 17, the robot climbed the pipe vertically with a wired power supply. In the test, the control and communication systems worked normally, and the robot could complete the preset locomotion gait. During the course of locomotion, the RMMs could anchor in the pipe reliably without any slippage, and the AMM also worked smoothly. The fastest measured speed of the robot was 2.9 mm/s when it was ascending and 3.3 mm/s when it was descending; the speed could be adjusted in the commands by inserting a time interval between every locomotion gait.

To verify locomotion capability in a real intestinal environment, an *in vitro* experiment was conducted. A section of porcine small intestine sampled from a 60 kg pig through a humane surgical approach was used for our test; its diameter ranged from 16 mm to 18 mm. The experimental method is shown in Fig. 18. Two ends of the small bowl were fixed on a shelf that allowed the route of locomotion to droop naturally. The route could be divided into three parts according to their angles: downhill, basically even, and uphill paths; the gradient ranged between -30°~+30°. During the experiment, the robot used a wired power supply. The average speed was 1.2 mm/s for the downhill route, 0.7 mm/s for the basically even route, and 0.3 mm/s for the uphill route. The locomotion efficiency was clearly inversely proportional to the gradient of the locomotion path.

4.4 Verification of the wireless power system

To verify the feasibility of the wireless power system and the performance of the robot in a strong-magnetic-field environment, a set of experiments were carried out. First we wound the coil and connected it to the resonance and rectifying circuit. Then the output of the rectifying circuit was connected to the control circuit, which included the voltage regulator circuit. However, at the very start we found that the robot could not work with the wireless power system. We found out the reason was that the large starting current of the coreless DC motor (up to 500 mA) decreased the system's voltage to less than 1.8 V

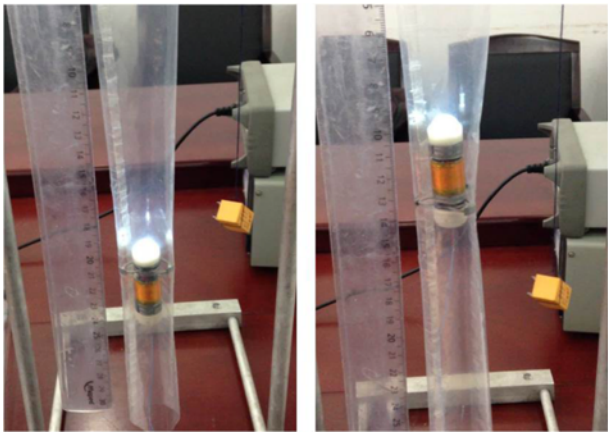

Fig. 17 Locomotion test in flexible pipe

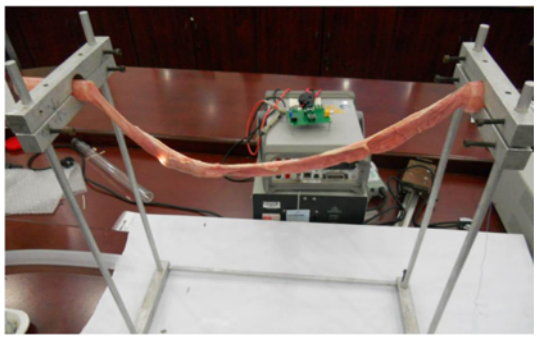

Fig. 18 Locomotion test in excised intestine

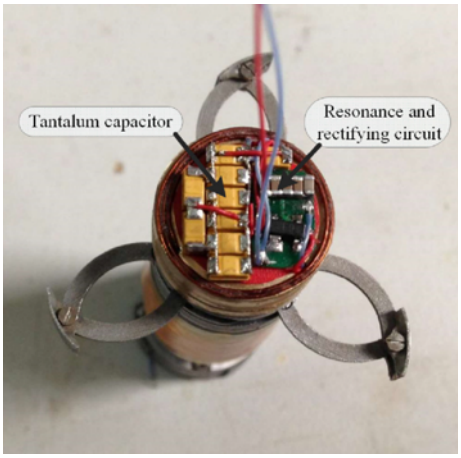

Fig. 19 The circuit of the wireless power receiving module

(minimum working voltage of the MCU), and caused the MCU to stop working. Although the starting time of the motor was just about 50 ms, the receiving power of the wireless power system and the capacitor of the voltage regulator (10 μF, reference value provided by voltage regulator chip) were insufficient to enable the robot to spend the overcurrent time with the voltage always exceeding 1.8 V. In light of the power limitations because of the restrained space of the coil, we enlarged the capacitor of the voltage regulator. As shown in Fig. 19, nine tantalum capacitors were added to the circuit, and each had a capacitance of 100 μF. After the modification, the robot could work stably with the wireless power system.

Fig. 20 shows the *in vitro* experiment with the wireless power system. Because the circuit was protected by a shield preventing

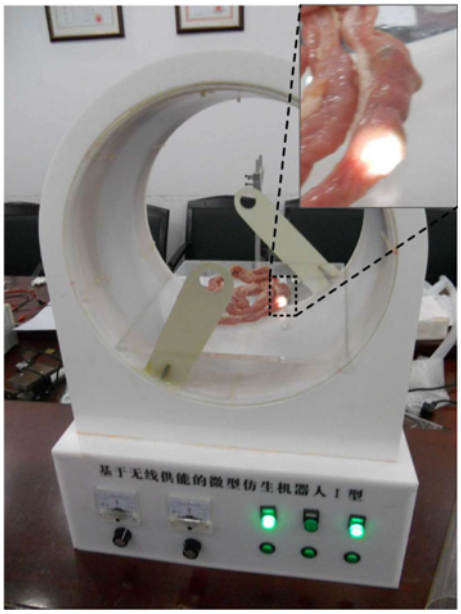

Fig. 20 Verification of the wireless power system

electromagnetic interference, the communication module could function when the transmission power was 20 W, and the control system could also work normally under the wireless power system. In addition, normal operation of the robot under various gait could be realized through external control. The results showed that the *in vitro* intestine didn't affect the wireless power receiving of the robot and the normal operation of the wireless communication.

5. Discussion and Conclusions

We designed, fabricated, and tested an expanding-extending robotic endoscope for active intestinal diagnosis. The robot measured Φ14×45 mm, including a receiving module for the wireless power system, a control system, and a video module. It is a very small one among the current inchworm-like robotic endoscopes that could be located by the authors. Although there were some on-board driven active endoscopes with single sections that had a smaller volume, but the hook-like [17] and thorn-like [19] legs may threaten the security of the intestinal wall (puncture). We designed an original RMM with three legs that extended along with the normal direction of the capsule's cross section. The three legs expanded in a closed curve to prevent entrapment of intestinal tissue; they could extend up to 32 mm in diameter to accommodate variable intestinal diameters.

A control system was designed based on the robot's features; for the coreless DC motor, a double feedback control was adopted. These provided feedback on the current of the motor and the position of the motion mechanism. The position detectors enhanced the stability of the mechanism while simultaneously reducing the power consumption of the system. To ensure the robot could work for a long time off-line, we designed a wireless power system to match the mechanical structure of the robot. With an effective wireless power system, the robot could detect the entire intestinal tract. We tested the prototype's performance (including mechanical properties, locomotion ability, and other parameters), which proved the feasibility of the robot. However, some points require additional attention:

(1) Although we attempted to shrink the robot's size, the prototype was still larger than expected. In our robot, the mechanism, circuit, and video module were 27 mm, 8 mm, and 10 mm in length, respectively, and every part was compressible to a certain extent, especially the length of the mechanism. If the robot crawled in the real human intestinal tract, the influence of the robot's length to locomotion mainly embodied in the location of intestinal bend especially a sharp one. Although the intestinal tract is soft and deformable, anchoring failure due to intestinal resistance increasing and locomotion efficiency reduction due to greater deformation of intestinal tract may occur in the process of robot locomotion when get through the bending of the gut. We will carry out *in vivo* experiment to verify this influence in our future research. If the result shows that the length of the robot seriously influence the locomotion in intestinal bend, we will consider to add a universal joint in the middle of the robot to reduce this influence.

(2) Given the limited space, the receiving coil of the wireless power system was one-dimensional. If the transmitting coil was also one-dimensional, the robot would not be able to operate in every direction. Two methods could resolve this issue: first, make a three-dimensional transmitting coil that fits the space size; second, expand the space to make a three-dimensional receiving coil. Because of the importance of maintaining the robot's volume, the first method would be preferable.

(3) The present study represents our first *in vitro* experiment related to this device. Although the *in vitro* experiments showed that the robot could effectively move in the gut, we were not sure to obtain the same results in the *in vivo* environment. Our future work will expand these *in vivo* experiments.

ACKNOWLEDGEMENT

In this paper, the research was sponsored by the National Natural Science Foundation of China (NSFC) (No. 31170968).

REFERENCES

1. Valdastri, P., Simi, M., and Webster III, R. J., "Advanced Technologies for Gastrointestinal Endoscopy," Annual Review of Biomedical Engineering, Vol. 14, pp. 397-429, 2012.
2. Cuschieri, A. and Melzer, A., "The Impact of Technologies on Minimally Invasive Therapy," Surgical Endoscopy, Vol. 11, No. 2, pp. 91-92, 1997.
3. Menciassi, A., Quirini, M., and Dario, P., "Microrobotics for Future Gastrointestinal Endoscopy," Minimally Invasive Therapy & Allied Technologies, Vol. 16, No. 2, pp. 91-100, 2007.
4. Moglia, A., Menciassi, A., Schurr, M. O., and Dario, P., "Wireless Capsule Endoscopy: From Diagnostic Devices to Multipurpose Robotic Systems," Biomedical Microdevices, Vol. 9, No. 2, pp. 235-243, 2007.
5. Iddan, G., Meron, G., Glukhovsky, A., and Swain, P., "Wireless Capsule Endoscopy," Nature, Vol. 405, No. 6785, pp. 417-417, 2000.

6. Meltzer, A. C., Ali, M. A., Kresiberg, R.B., Patel, G., Smith, J. P., et al., "Video Capsule Endoscopy in the Emergency Department: A Prospective Study of Acute Upper Gastrointestinal Hemorrhage," Annals of Emergency Medicine, Vol. 61, No. 4, pp. 438-443, 2013.

7. Ciuti, G., Menciassi, A., and Dario, P., "Capsule Endoscopy: From Current Achievements to Open Challenges," IEEE Reviews in Biomedical Engineering, Vol. 4, pp. 59-72, 2011.

8. Zhou, H., Alici, G., Than, T. D., and Li, W., "Modeling and Experimental Characterization of Propulsion of a Spiral-Type Microrobot for Medical Use in Gastrointestinal Tract," IEEE Transactions on Biomedical Engineering, Vol. 60, No. 6, pp. 1751-1759, 2013.

9. Yim, S. and Sitti, M., "Design and Rolling Locomotion of a Magnetically Actuated Soft Capsule Endoscope," IEEE Transactions on Robotics, Vol. 28, No. 1, pp. 183-194, 2012.

10. Lee, J. S., Kim, B., and Hong, Y. S., "A Flexible Chain-based Screw Propeller For Capsule Endoscopes," Int. J. Precis. Eng. Manuf., Vol. 10, No. 4, pp. 27-34, 2009.

11. Hong, Y. S., Kim, J. Y., Kwon, Y. C., and Song, S. Y., "Preliminary Study of a Twistable Thread Module on a Capsule Endoscope in a Spiral Motion," Int. J. Precis. Eng. Manuf., Vol. 12, No. 3, pp. 461-468, 2011.

12. Chen, W., Yan, G., Wang, Z., Jiang, P., and Liu, H., "A Wireless Capsule Robot with Spiral Legs for Human Intestine," The International Journal of Medical Robotics and Computer Assisted Surgery, Vol. 10, No. 2, pp. 147-161, 2014.

13. Park, H. J., Kim, D., and Kim, B., "A Robotic Colonoscope with Long Stroke and Reliable Leg Clamping," Int. J. Precis. Eng. Manuf., Vol. 13, No. 8, pp. 1461-1466, 2012.

14. Lin, W., Shi, Y., Jia, Z., and Yan, G., "Design of a Wireless Anchoring and Extending Micro Robot System for Gastrointestinal Tract," The International Journal of Medical Robotics and Computer Assisted Surgery, Vol. 9, No. 2, pp. 167-179, 2013.

15. Ito, T., Kito, Y., Ishimori, S., Phunopas, A., and Hayashi, T., "Capsule Micromechanism Driven by Impulse," Micromechanics and Microactuators, pp. 11-22, 2012.

16. Gao, P., Yan, G., Wang, Z., Wang, K., Jiang, P., and Zhou, Y., "A Robotic Endoscope based on Minimally Invasive Locomotion and Wireless Techniques for Human Colon," The International Journal of Medical Robotics and Computer Assisted Surgery, Vol. 7, No. 3, pp. 256-267, 2011.

17. Valdastri, P., Webster, R. J., Quaglia, C., Quirini, M., Menciassi, A., and Dario, P., "A new mechanism for mesoscale legged locomotion in compliant tubular environments," IEEE Transactions on Robotics, Vol. 25, No. 5, pp. 1047-1057, 2009.

18. Wang, K., Yan, G., Jiang, P., and Ye, D., "A Wireless Robotic Endoscope for Gastrointestine," IEEE Transactions on Robotics, Vol. 24, No. 1, pp. 206-210, 2008.

19. Quirini, M., Menciassi, A., Scapellato, S., Stefanini, C., and Dario, P., "Design and Fabrication of a Motor Legged Capsule for the Active Exploration of the Gastrointestinal Tract," IEEE/ASME Transactions on Mechatronics, Vol. 13, No. 2, pp. 169-179, 2008.

20. Terry, B. S., Lyle, A. B., Schoen, J. A., and Rentschler, M. E., "Preliminary Mechanical Characterization of the Small Bowel for in Vivo Robotic Mobility," Journal of Biomechanical Engineering, Vol. 133, No. 9, Paper No. 091010, 2011.

21. Lyle, A. B., Luftig, J. T., and Rentschler, M. E., "A Tribological Investigation of the Small Bowel Lumen Surface," Tribology International, Vol. 62, pp. 171–176, 2013.